LA-UR-12-26232
Approved for public release; distribution is unlimited.

Title:	Differential Die-Away Self-Interrogation for Treaty Verification Applications
Author(s):	Henzl, Vladimir Menlove, Howard O. Thron, Jonathan L.
Intended for:	Report

Final Report: **Nov 2012**

Differential Die-Away Self-Interrogation for Treaty Verification Applications

Vladimir Henzl, Howard O. Menlove, and Jonathan Thron
Los Alamos National Laboratory

Abstract:

In this report, we summarize our experimental and simulation study of Differential Die-Away Self-Interrogation (DDSI) method used to assay 4 PuO_2 samples of almost identical isotopic composition with total Pu content ranging from 60-614g. With measured and calculated traditional neutron coincidence rates such as singles (S), doubles (D) and triples (T) we explore three different proposed DDSI signatures (D/S, T/S and D_L/D_F) over a wide range of gating scenarios and analyze the sensitivity of individual observables to fissile content of the sample. We find that only the D_L/D_F observable is exclusively sensitive to the fissile content of sample, while D/S and T/S yield sensitivity to both fertile and fissile component of the sample. Based on the results of the Monte Carlo simulations, depending on the mass of the PuO_2 sample and considering 900s assay time with the Epithermal Neutron Multiplicity Counter (ENMC) we are able to reconstruct the fissile content with statistical uncertainty of 0.4-3.7% in case of D/S ratio, 1.1-4.3% in case of T/S ratio, and 4.9-34.3% in the case of the D_L/D_F.

Introduction to DDSI concept

The main principle of Differential Die-Away Self-Interrogation (DDSI) method is very similar to that of the traditional Differential Die-Away (DDA) [1]. However, instead of external pulsed neutron source as in the case of DDA, the DDSI based instrument uses the spontaneously fissioning nuclei (primarily ^{240}Pu) of the assayed sample to produce interrogating neutron "time pulses", which induce fission on present fissile isotopes such as ^{239}Pu, ^{241}Pu and ^{235}U.

When neutrons are released during a spontaneous fission of a nucleus of a fertile isotope they may induce fast fission of another fissile nucleus present in the sample, reflecting thus its multiplication factor, given by the mass, and chemical and physical composition. However, in traditional applications of passive neutron coincidence counting techniques the multiplication factor of assayed samples are low, thus the count rate of detected neutrons is closely proportional to the amount of spontaneously fissioning nuclides such as ^{240}Pu and ^{242}Pu. The content of fissile isotopes such as ^{239}Pu and ^{241}Pu is then usually extrapolated from known isotopic composition, and the coincidence measurement of the ^{240}Pu effective.

On the other hand, the DDSI method, first proposed in [2], takes advantage of these fast neutrons released from the sample primarily by the fertile isotopes. We have added a polyethylene cylinder surrounding the assayed sample to act as a moderator as well as a reflector returning the (now already thermalised) neutrons back into the sample where, due to their low energy, only fissile isotopes are now prone to induced fission. A second population of fast neutrons is then created that can cause fast-neutron multiplication, can emerge from the sample to be either thermalised and returned again to the sample, or can escape from the surrounding polyethylene cylinder and be ultimately detected.

While the die-away time of the original fast neutron population (τ_{fast}) is short and depends on the detector die-away (τ) , the die-away time of the neutron population created by induced fission of fissile isotopes by thermalised neutrons is much longer (τ_{therm}), thus creating opportunity to directly measure the presence of fissile isotopes in the assayed sample by employing just slightly modified coincidence counting scheme similar to those employed in traditional passive neutron coincidence counting techniques.

The **Fig.1** schematically displays a typical Rossi-Alpha distribution for a sample undergoing assay using a DDSI instrument. "Fast" and "slow" component of the distribution reflect the vastly different die-away times of the two neutron populations created either by spontaneous or induced fission. The indicated "fast" and "late" time domains then display how selecting a properly delayed gate for traditional neutron coincidence counting may change our sensitivity from fertile to fissile content of the sample.

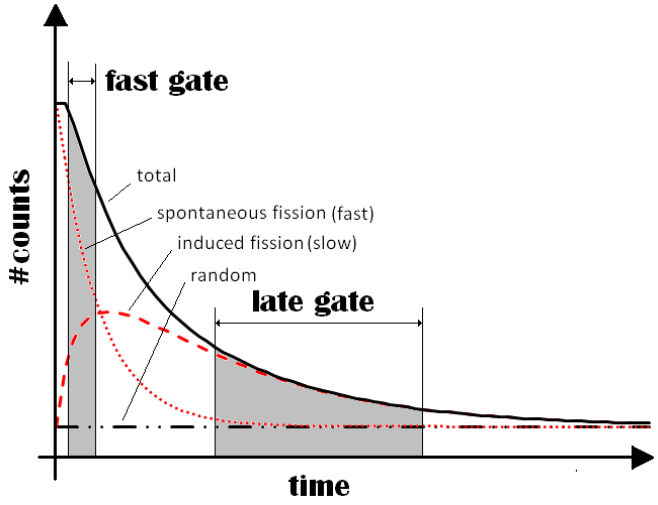

Fig.1 *Typical Rossi-Alpha distribution of a sample assayed by a DDSI instrument with indicated contributions by different processes*

While, in general, the main principles of the DDSI concept have already been demonstrated for spent fuel [2], its practicality, and usability for various purposes such as plutonium verification, remains to be explored and verified. Within the subsequent sections we explore experimentally, as well as by means of Monte Carlo simulations, several aspects of the DDSI method for potential use for plutonium

measurements in treaty verification applications, where, in general, kilogram quantities of plutonium are expected to be present.

The experimental approach using the ENMC

Since no dedicated DDSI instrument has been built, for the purposes of this study, we have taken advantage of a well known and established Epithermal Neutron Multiplicity Counter (ENMC) [3] modified by custom-made high-density polyethylene (HDPE) container inserted inside the sample cavity of the ENMC detector, and housing the samples to be assayed. The HDPE container was in the form of a hollow cylinder with height of 280mm and diameter of 190mm, while the height and diameter of its inner cavity was 172mm and 130mm, respectively (see **Fig.2**)

In this study, we have used four plutonium oxide samples of very similar isotopic composition varying only by their total mass, as stated in **Table 1**, where $^{239}Pu_{eff}$ is defined analogous to $^{240}Pu_{eff}$ as a weighted sum of all fissile isotopes present in the sample, i.e. $^{239}Pu_{eff}$ =m(^{239}Pu)[g]+1.326·m(^{241}Pu)[g].

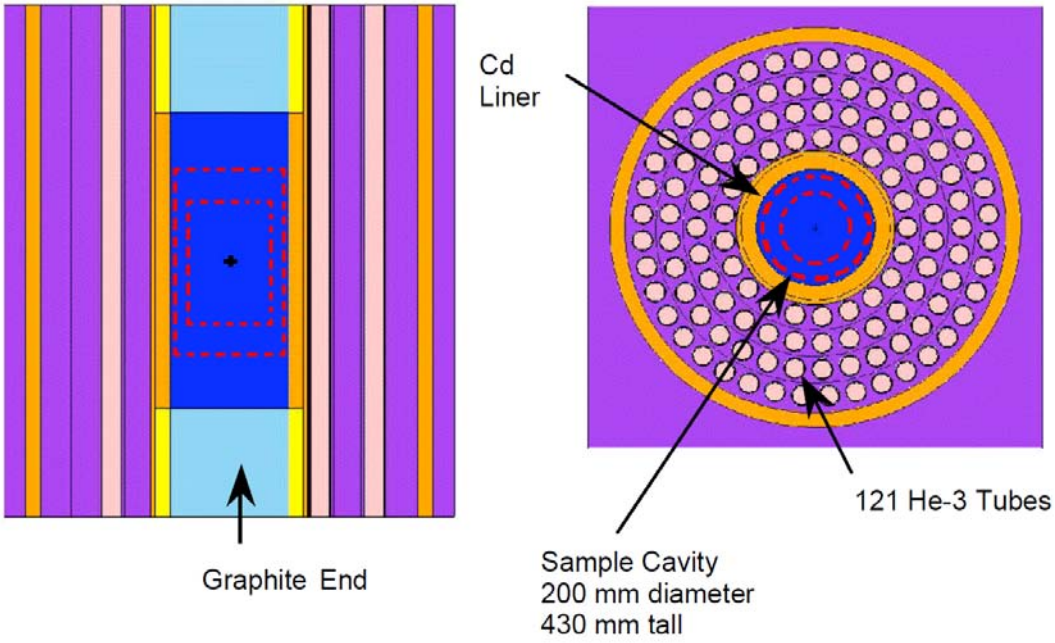

Fig.2 *Diagram of the ENMC showing the layout of the ^{3}He tubes in the HDPE detector body separated by a Cd liner from the sample cavity. The red dashed lines indicate the location of the additional HDPE container responsible for the DDSI effect.*

Table 1 *Declaration of isotopic composition of SNM samples used in the current study (declaration date 4/18/2011)*

		Isotopic values in weight %								
Item	**Total Pu mass [g]**	**^{238}Pu**	**^{239}Pu**	**^{240}Pu**	**^{241}Pu**	**^{242}Pu**	**^{241}Am**	**$^{240}Pu_{eff}$ fraction**	**$^{240}Pu_{eff}$ [g]**	**$^{239}Pu_{eff}$ [g]**
LAO250	59.37	0.0473	82.9653	16.3045	0.3454	0.3375	1.0337	0.170	10.09	49.53
LAO251	170.15	0.0530	82.7654	16.4802	0.3536	0.3477	1.0662	0.172	29.26	141.62
LAO255	538.27	0.0571	82.8681	16.3859	0.3454	0.3436	1.0337	0.171	92.08	448.52
LAO253	606.61	0.0465	82.7531	16.4979	0.3427	0.3598	1.0411	0.172	104.45	504.75

The PuO_2 was in the form of a powder that has triple encapsulation in a stainless steel can with the inner most diameter being 82.5mm, and the outermost diameter being 163mm. The PuO_2 powder thus took a geometrical form of a pancake at the bottom of the inner most can. Assuming the average density of the PuO_2 of 2.0 $g.cm^{-3}$, the thickness of the oxide layer was estimated to be 0.64, 1.85, 6.58, and 5.84 cm in case of the LAO250, LAO251, LAO253, and LAO255 samples, respectively.

The experimental measurements analyzed within this report took part in January 2012 during the IAEA school at Los Alamos in TA-35, when safety and security requirements were met to allow for programmatic work with Cat. III special nuclear material (SNM) samples. However, the limited window of opportunity allowed for only one set of assays of all four sources with an HDPE moderator (i.e. DDSI condition) and only a single assay of one source (LAO253) in a bare geometry, representing thus a regular neutron coincidence measurement.

All performed assays consisted of 30 cycles of 30s duration (i.e. 900s live time total), which corresponds to a practical approach suitable for treaty verification purposes. The data acquisition (DAQ) system complementing the ENMC detector employed two branches; the first one being the shift register branch using a standard JSR-15 multiplicity shift register with preset predelay (PD) of 1.5μs and gate width (G) of 24μs, while the second branch consisted of PTR-32 list-mode electronic module where PD and G width is defined in the subsequent data post-processing. While both DAQ branches were active in parallel at the same time, they essentially ran independently of each other, and their results (though statistically equal) are thus not exactly the same. The reason we chose such DAQ architecture was to verify performance of the novel list-mode branch by the traditional shift-register branch, since only the list-mode data can be analyzed offline using any user defined gate width that is necessary for exploration of possible DDSI signatures.

The **Table 2** compares and summarizes results of the measurements in terms of rates of singles, doubles and triples measured by each branch of the data acquisition system with PD=1.5μs and G=24μs. The results presented in the table clearly confirm the agreement between the two DAQ branches, allowing us now to concentrate fully on the results from the list-mode data analysis which provides the flexibility needed for the exploration of the expected DDSI signatures. Unless explicitly stated, the experimental results presented in any of the subsequent sections were acquired with the list-mode branch of the DAQ, i.e. using the PTR-32 list-mode electronic module.

Table 2 *Results of assay of LAO sources with shift register and list-mode branch of the DAQ; ΔS, ΔD, and ΔT are relative statistical uncertainties of S, D, and T, respectively.*

	Shift register analysis						List-mode analysis					
Item	S [cps]	ΔS [%]	D [cps]	ΔD [%]	T [cps]	ΔT [%]	S [cps]	ΔS [%]	D [cps]	ΔD [%]	T [cps]	ΔT [%]
LAO250	7082.58	0.04	1132.827	0.24	181.651	1.00	7082.01	0.05	1131.94	0.23	181.728	0.93
LAO251	21319.33	0.02	3843.124	0.09	726.739	0.38	21321.0	0.01	3846.23	0.09	728.653	0.39
LAO253	81926.97	0.02	18345.622	0.13	4822.806	0.78	81889.6	0.02	18377.5	0.14	4847.28	0.47
LAO255	71412.88	0.02	15605.915	0.14	3961.607	0.73	71413.1	0.01	15659.2	0.15	3979.33	0.63

In the traditional, passive-neutron coincidence-counting method, the measured doubles rate (D), enhanced by the fast multiplication, correlates with the effective mass of ^{240}Pu. The left panel of **Fig.3** displays how D increases with the increasing $^{240}Pu_{eff}$ and the length of the gate (PD=1.5μs in all cases displayed in Fig.3). Should we proceed with the traditional analysis, the nonlinear trend of the D as function of $^{240}Pu_{eff}$ would be corrected by known multiplication to result in linear dependency of D on $^{240}Pu_{eff}$. However, due to the presence of the HDPE cylinder, the D rate is influenced not only by the fast multiplication, from the first generation of neutrons from spontaneous fission, but is also enhanced by the thermal multiplication due to the moderated neutrons returned back into the sample. Point model assumptions are thus no longer valid, and analysis tools such as INCC code may fail to determine overall multiplication factors correctly. In order to illustrate the presence of the M_{th} that is realized generally later than the M_F we have normalized the D rates to those of the shortest gate and the smallest PuO_2 sample as in right panel of Fig.3. The steeper trend of D for assays with longer gates implies higher overall multiplication, with the difference being made in later times within the gate, consistent with our hypothesis of M_{th}.

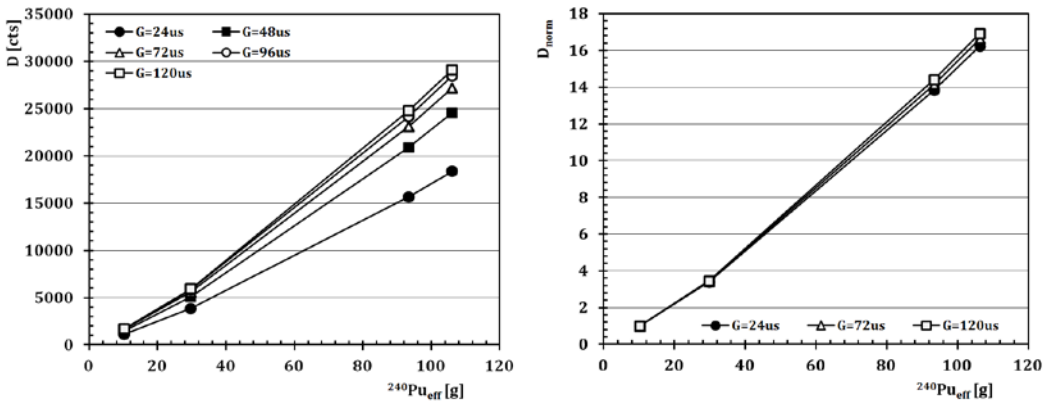

Fig.3 *Experimentally detected doubles rate (left) and normalized doubles rate (right) as the function of the $^{240}Pu_{eff}$.*

Within the DDSI approach, as already suggested in [2], the new signatures arise from the thermal multiplication of the sample created by the neutron-albedo effect due to an additional HDPE cylinder surrounding the assayed sample. Fig.1 showed that the choice of a counting time interval has a detrimental effect on the origin of the detected neutrons. Therefore in order to create a quantity exclusively sensitive to the thermal multiplication, the chosen gate has to be late enough that most of the fast neutron population has already died out. However, the fission induced by thermal neutrons leads to a production of correlated fast neutrons, thus enhancing the count rate in the early time domains as well, and potentially leading to a signature sensitive to both fertile and fissile content of the sample. In most cases, the quantitative evaluation of the most suitable gate width and delay is far from trivial and depends clearly on the definition of the DDSI signature. For the purposes of this report we decided to explore three different observables: D/S, T/S and D_L/D_F where S stands for detected rate of singles, D doubles, T triples and indices L and F for late and fast, indicating the time domain of the gate in which the doubles rate was measured.

Both D/S and T/S observables will be first explored by changing PD between the start of the event and the opening of a gate in order to characterize its sensitivity to increasing mass of the Pu in the sample. With respect to the $D_L/D_{F,}$ we have to consider that the die-away time of the fast neutrons from spontaneous fission should not be affected by the presence of the HDPE block, and is in case of the ENMC detector ~22μs. The width of the fast gate will therefore be set to 24μs with PD of 1.5μs as is the standard for this type of the detector without its DDSI modification. In contrast, the introduction of the HDPE container around the assayed samples results in significant thermal-neutron multiplication with a die-away time of ~60μs. We will therefore explore the sensitivity of the observable by varying the width of the slow gate, as well as its delay with respect to the fast gate.

The left panel of **Fig.4** displays ratio of doubles to singles, D/S, as measured for four PuO_2 samples with gate width set to 24 μs and the PD set to (1.5+n16) μs, where n=0,1,2,3,4,5. The central panel of Fig.2 displays ratio of triples to singles, T/S, under same gate conditions as in case of D/S. The right panel display D_L/D_F ratio with fast gate being 24μs wide, with standard PD of 1.5 μs, and late gate being 24 or 64 μs wide and delay with respect to the end of the fast gate by 0, 32, and 64 μs. All of the three quantities are plotted against the fissile content of the PuO_2 samples represented by $^{239}Pu_{eff}$.

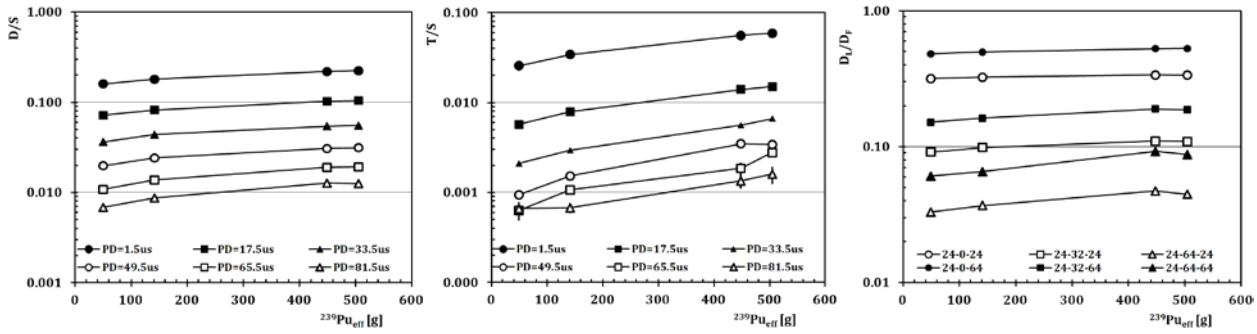

Fig.4 *Experimental results of three proposed DDSI signatures (D/S, T/S, and D_L/D_F) as the function of the effective fissile content of the PuO_2 samples assayed with variable PD and constant G (error bars, when larger than the data points, indicate statistical uncertainty).*

The left panel of Fig.4 indicates that D/S increases with the mass of the fissile content in the PuO_2 samples, for any of the chosen PD's. Additionally, considering the logarithmic scale of the y-axis, the changing slope of the depicted lines suggests that the sensitivity of this observable increases with longer PD, even though the absolute magnitude decreases. However, the flattening of the dependencies with increasing $^{239}Pu_{eff}$ suggests considerable self-shielding effects, which seem to be more pronounced in case of the longer PD. The thermal neutron self-shielding is mitigated by the fast-neutron multiplication that shows up in the shorter time intervals. Thus, the long PD's have the self-shielding effect and are not good choices for the DDSI method.

The central panel of Fig.4 demonstrates that T/S also is a quantity apparently correlated with the total fissile content in the PuO_2 samples. Moreover, it seems the sensitivity of the signal is even larger than in case of D/S. However, the T/S ratio loses the statistical precision with increasing PD time interval because most of the correlations are in the early time intervals. A better approach thus may be to

evaluate the T ratio with a short gate in place of the PD, and then subtract the short gate from the long gate for the net T. In general, the statistical uncertainty can of course be reduced by prolonged measurement, yet depending on the specific conditions of the use of the instrument long enough assays may not be deemed practical.

The right panel of Fig.4 displays how D_L/D_F evolves with increased fissile content in the sample and how this particular observable depends on the choice of DDSI delay and the width of the late gate. In general, the data provide clear indication that with longer late gate the magnitude of the signal is larger, which implies improved statistics, thus higher accuracy. The longer the DDSI delay, i.e. the separation between the two gates, the more sensitive the observable to $^{239}Pu_{eff}$, although the sooner (in terms of $^{239}Pu_{eff}$ mass) it reaches saturation, presumably due to the self-shielding effects in large samples.

In general, the results in Fig.4 seem to suggest that all three of the chosen observables yield sensitivity to the total fissile content in the sample, although with long PD's the presumed self-shielding effects may limit the applicability to only "small enough" samples. Such limits seem to depend on the parameters of the chosen gate(s) and the complementary PD or DDSI delay, but in reality may also depend on the chemical, isotopic and physical composition of the assayed sample. Should we consider that the "self-interrogation" caused by the additional HDPE container is performed by predominantly thermal neutrons, we can easily imagine their limited penetrability in case of Pu metal. For metal samples and high mass oxides it will be better to use long gates with short pre-delays to obtain both the strong fissile response combined with the fast-neutron multiplication boost in the early time period to mitigate the thermal-neutron self-shielding. Therefore in **Fig.5** we display the same observables as in Fig.4 (D/S, T/S and D_L/D_F) yet this time the PD is chosen to be 1.5us in all displayed scenarios, and only the length of the gate varies.

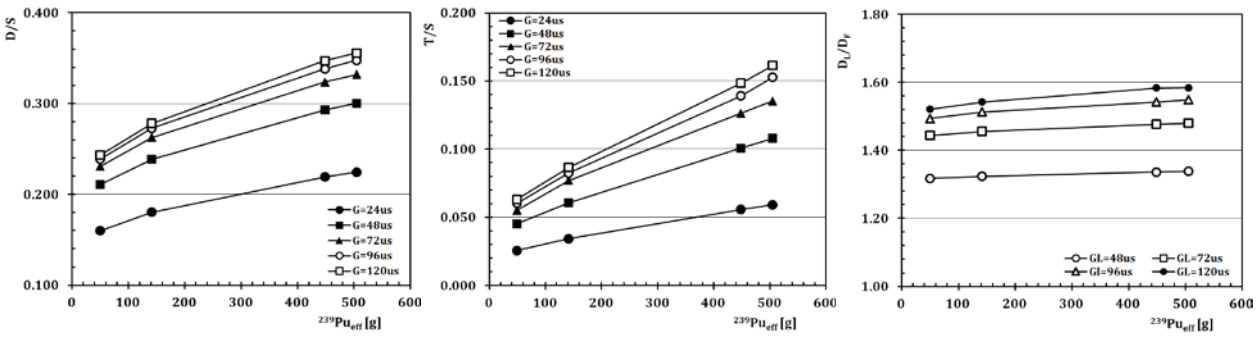

Fig.5 *Experimental results of three proposed DDSI signatures (D/S, T/S, and D_L/D_F) as a function of the effective fissile content of the PuO_2 samples assayed with constant PD and variable G (error bars indicating the statistical uncertainty are smaller than the data points).*

Unlike in Fig.4, the results in Fig.5 do not exhibit such strong self-shielding saturation. These results thus support our choice of longer gates with short PD's rather than short gates with long PD's, even though the curvature of the trends in all three panels suggests a presence of minor self-shielding effects as well.

Additionally, the correlation of the three observables, both in Fig. 4 and 5, with $^{239}Pu_{eff}$ mass should not be considered a proof of sensitivity exclusively to the fissile content in the sample. Since in our case the isotopic composition of all four samples was nearly identical, then in the same proportion as the fissile content rises with total mass of PuO_2, so does the total mass of ^{240}Pu. Without additional information it is thus impossible to distinguish whether the trends in Fig. 4 and 5 are caused by increased fertile or fissile content. In order to understand how the chosen observables (D/S, T/S and D_L/D_F) dependent on fissile and/or fertile content we need to verify how these observables perform without the self-interrogation effect, i.e. without the HDPE cylinder present. Unfortunately, the single measurement in "bare" geometry with LAO253 sample is not enough to evaluate the sensitivity of these observables to the amount of fissile or fertile material, and without the ability to complement already performed measurements with additional experimental tests we will resort to Monte Carlo simulations.

Monte Carlo simulations

If properly benchmarked, Monte Carlo simulations can be a powerful tool to explore and gain insight into complex physics phenomena such as DDSI. Due to the novel nature of the investigated method such additional tools may be of a particular value to help understand which time domains and what gate lengths may be the most sensitive to the presence of the fissile material, and/or help us evaluate various proposed observables.

We have therefore used MCNPX [4] code to simulate the neutron coincidence rates registered by the ENMC detector under as close as possible conditions to the conditions under which the real experimental measurement was performed. To the best of our knowledge we have modeled the exact experimental setup, including the triple encapsulation of the PuO_2, HPDE container and the complex geometry of the ENMC detector.

In the first step, for each of the four samples we have simulated as many spontaneous fission events as there would be created in a sample during 900s life-time assay. Thus, the statistics of the simulations could be directly compared to the experimental data. However, rather than using coincidence tallies, which require preset PD and G, the simulated histories (i.e. the fate of neutrons from individual spontaneous fission) were written into a ptrac file, which can be subsequently used to create a pulse train similar to experimental pulse trains acquired by the list-mode DAQ. The offline analysis of the simulated pulse trains thus profits from the identical flexibility as the offline analysis of the list-mode data.

Following the conclusion of the previous section we will simulate an assay of the samples comparable with the results displayed in Fig. 5, i.e. assay scenarios with short and constant PD (=1.5μs) and variable gate length (G=24, 48, 72, 96, and 120μs).

The **Table 3** summarizes measured and simulated rates of S, D, and T in case of 24μs gate, **Table 4** then summarizes measured and simulated rates of the same quantities with a gate width of 120μs. **Table 5** provides ratios of the experimental to simulated values.

Examining the results in Table 5, the high values of S_{exp}/S_{sim}, in the ratios only reflect the presence of (α,n) reactions in the sample that was omitted in the simulations. With α coefficient being known

(~0.51) for all four samples, it can be verified, that the S rates in experiment and simulations do not differ by more than 5%. However, the match between D and T rates is regarded as more important for the comparison, since these two rates are more sensitive to the multiplication of the sample enhanced by the detector setup, particularly by the HDPE container. The D_{sim} is within 1-2% of D_{exp} consistently over the full range of the PuO_2 masses used in this study, if the short G of 24μs is used in the analysis. For the same G, the difference between simulated and experimental rates of triples is also only off by about 1-3%, which is considered a very good agreement.

The situation changes if G of 120μs is chosen in order to make the coincidence rates rather more sensitive to the thermal multiplication enhanced by the presence of the HDPE sleeve. The difference between the doubles rates increases to ~5% and reaches ~ 11% in case of the triples rate. In both cases, it is the simulation which results in higher coincidence count rates, reflecting slower die-away time in the model than in the reality, presumably overestimating the DDSI effect.

Identification of the exact source of the discrepancy may require additional, and more detailed, study, however, considering experience and basic understanding of the underlying physical processes, we may speculate about the uncertainty of the known density of the PuO_2 powder and its geometry as being the prime suspects. It indeed has been found in the past that our assumed density of 2 $g.cm^{-3}$ has not led to the best match between simulations and the experiment [5]; moreover this density may in principle vary from sample to sample between approximately 2-4 $g.cm^{-3}$. Should the density be different, the geometry of the sample would need to be adjusted, which in turn may influence the multiplication of the sample. While the simulated results may not prove to be a good match on an absolute scale for the extended gates, the qualitative trends of the simulations may still provide valuable guidance in our understanding of the experimental results, especially in the comparison of “bare” vs. “DDSI” geometry of the detector setup. The left panel of **Fig. 6** displays the net multiplication as observed in the simulations for both of these geometries, while the central and the right panels display D and normalized D rates acquired with 24μs and 120μs gates and how they differ with choice of the assay geometry.

The net multiplication calculated in MCNPX should not be confused with leakage multiplication typically used/calculated by neutron coincidence counting analysis codes such as INCC. Moreover, INCC uses point model equations in its evaluation of leakage multiplication, but the setup with a reflective geometry used to create the DDSI effect is in violation of these principles, thus preventing a direct comparison of experimental multiplication with the simulated one. Nevertheless, the results in the left panel of Fig.6 clearly indicate that the addition of the HDPE block significantly increases the multiplication of the setup, presumably by the DDSI effect. The same conclusion can be drawn from the right panel of the Fig.6. In bare geometry, the multiplication of the samples is low, thus the trends of D_{norm} are almost linear. However, the increased multiplication due to the addition of the HDPE bloc results in curvature of the trends in the same plot for the D_{norm} values calculated in DDSI geometry.

We can now compare the sensitivity of the proposed DDSI signatures (i.e. D/S, T/S, D_L/D_F) as used in the analysis of the experimental data above (i.e. comparable with Fig. 5). While quantitative comparison may be misleading, the qualitative differences may be the indicators of the underlying principles (i.e. fast or thermal multiplication of fertile or fissile material) behind the trends observed in Fig. 5.

Table 3 *PD=1.5μs, G=24μs*

	experiment						simulation					
Item	S [cps]	ΔS [%]	D [cps]	ΔD [%]	T [cps]	ΔT [%]	S [cps]	ΔS [%]	D [cps]	ΔD [%]	T [cps]	ΔT [%]
LAO250	7082.0	0.05	1131.9	0.23	181.73	0.93	4702.7	0.07	1158.6	0.18	182.4	0.77
LAO251	21321.0	0.01	3846.2	0.09	728.65	0.39	14274.8	0.04	3839.2	0.20	737.8	0.56
LAO253	81889.6	0.02	18377.5	0.14	4847.28	0.47	49227.7	0.02	15634.4	0.08	4069.8	0.63
LAO255	71413.1	0.01	15659.2	0.15	3979.33	0.63	56569.6	0.02	18347.3	0.13	4987.4	0.49

Table 4 *PD=1.5μs, G=120μs*

	experiment						simulation					
Item	S [cps]	ΔS [%]	D [cps]	ΔD [%]	T [cps]	ΔT [%]	S [cps]	ΔS [%]	D [cps]	ΔD [%]	T [cps]	ΔT [%]
LAO250	7080.8	0.049	1721.3	0.267	447.144	1.332	4702.7	0.07	1841.8	0.24	495.1	1.49
LAO251	21319.8	0.013	5930.33	0.170	1847.46	0.928	14274.8	0.04	6202.8	0.32	2069.3	1.09
LAO253	81888.3	0.014	29116.7	0.243	13220.3	1.413	49227.7	0.02	26014.3	0.19	12190.3	1.14
LAO255	71415.5	0.015	24797.1	0.248	10593.9	1.485	56569.6	0.02	30692.9	0.20	14832.9	1.31

Table 5 *ratio of experimental to simulated neutron coincidence rates*

	PD=1.5μs; G=24μs						PD=1.5μs; G=120μs					
Item	S_{exp}/S_{sim}	err [%]	D_{exp}/D_{sim}	err [%]	T_{exp}/T_{sim}	err [%]	S_{exp}/S_{sim}	err [%]	D_{exp}/D_{sim}	err [%]	T_{exp}/T_{sim}	err [%]
LAO250	1.51	0.08	0.98	0.29	1.00	1.20	1.51	0.08	0.93	0.36	0.90	2.00
LAO251	1.49	0.04	1.00	0.22	0.99	0.68	1.49	0.04	0.96	0.36	0.89	1.43
LAO253	1.45	0.03	1.00	0.16	0.98	0.89	1.45	0.03	0.95	0.31	0.87	1.87
LAO255	1.45	0.03	1.00	0.20	0.97	0.68	1.45	0.03	0.95	0.31	0.89	1.93

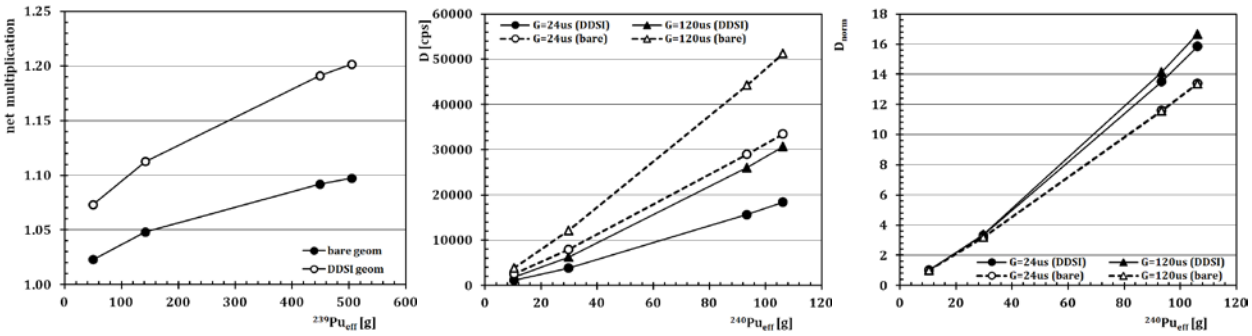

Fig. 6 *Net multiplication simulated by MCNPX for bare and DDSI detector geometry (left) as a function of the fissile content in the samples; Simulated doubles (center) and normalized doubles (right) rates as the function of $^{240}Pu_{eff}$ for DDSI and bare geometry with two different gate width scenarios.*

Fig. 7 is an exact analogy of Fig. 5, with the difference being that MCNPX simulated rather than experimental values of D/S, T/S and D_L/D_F are displayed for PD=1.5μs, various widths of G and G_L (with G_F=24μs), and DDSI delay. **Fig. 8** then displays identical simulated quantities as Fig. 7, this time, however, simulated in bare geometry, i.e. without the HDPE block surrounding the assayed samples.

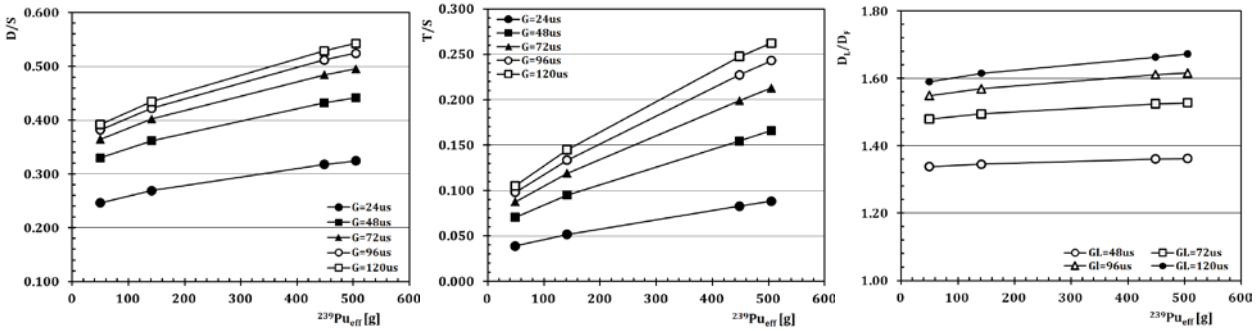

Fig.7 *Simulated values of three proposed DDSI signatures (D/S, T/S, and D_L/D_F) as the function of the effective fissile content of the PuO_2 samples using the DDSI geometry (error bars indicating the statistical uncertainty are smaller than the data points).*

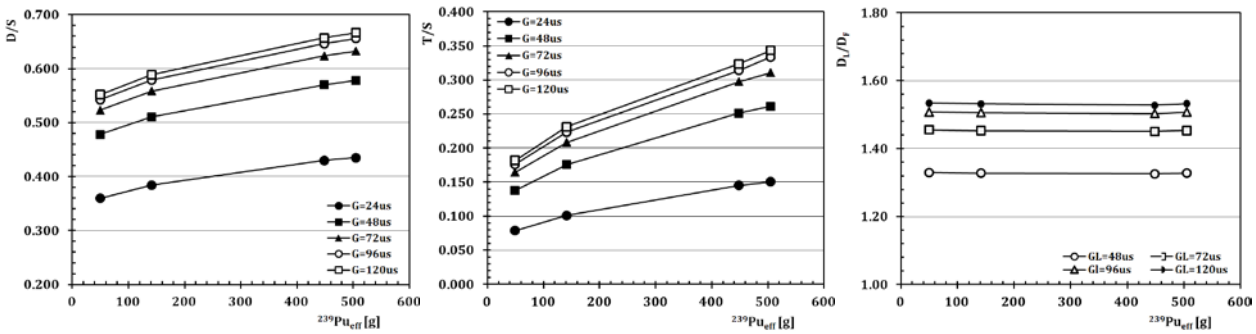

Fig.8 *Simulated values of three proposed DDSI signatures (D/S, T/S, and D_L/D_F) as the function of the effective fissile content of the PuO_2 samples using the bare geometry (error bars indicating the statistical uncertainty are smaller than the data points).*

Comparing first the simulated DDSI results in Fig. 7 to the experimental data depicted in Fig. 5 differences to be found do not seem qualitatively significant, although quantitatively they are influence by the absence of (α,n) reactions in the simulations. Somewhat surprisingly also the results in Fig. 8, which displays the values of the DDSI signatures calculated in bare geometry, seem to be qualitatively very similar to the experimental results in Fig. 5 as well as calculated values for the DDSI geometry in Fig. 7. The only notable exception is the D_L/D_F ratio, which in bare geometry does not seem to yield any sensitivity to the Pu content, should it be fertile or fissile isotopes or any combination of both. This is to be expected, because in the bare case there are no thermal neutrons to induce fission reactions in the late-time gate. Considering that the main difference between DDSI and bare geometries is the presence or absence of the thermal neutron flux (reflected back to the sample by the HDPE container) we can interpret the behavior of D_L/D_F as being typical of an observable that is exclusively sensitive to the

fission induced by thermal neutrons, i.e. the fissile content of the sample. On the other hand, the fact that D/S and T/S ratios scale with the $^{239}Pu_{eff}$ content even in bare geometry implicates that these observables are sensitive to both fissile as well as fertile content in the sample. **Fig. 9** displays the ratio of DDSI signatures as calculated for DDSI and bare geometries, while **Fig. 10** displays these double ratios normalized to the values calculated for the smallest PuO_2 sample. Fig. 9 documents how the absolute values of these ratios change with different choice of the gate width, and indeed the slope of the dependences reflect the increased sensitivity of the individual DDSI signature. But only the normalized values displayed in Fig. 10 provide for a direct comparison between different gating scenarios as well as different DDSI signatures. For example, from the left panel of Fig. 10 it can be concluded that the longer the gate the more sensitive the D/S ratio becomes to the Pu content in the DDSI geometry. The same holds true for the T/S ratio, but only for the shorter gates. With the longer gates the sensitivity of T/S to $^{239}Pu_{eff}$ seems to saturate for the samples with the highest masses. However, in general, it seems that T/S profits more from the DDSI effect than the D/S ratio (relative signal gain of 14% in case of D/S and 29% in case of T/S for the heaviest PuO_2 sample and longest gate width of 120µs). Compared to D/S and T/S the relative signal gains of D_L/D_F seem rather small (5% for the heaviest PuO_2 sample with G_L=120µs), however, as discussed above, its exclusive sensitivity to fissile content makes it a qualitatively different observable than D/S and T/S with potentially different applications, that may not be hindered by apparently lower relative signal gains in the DDSI configuration.

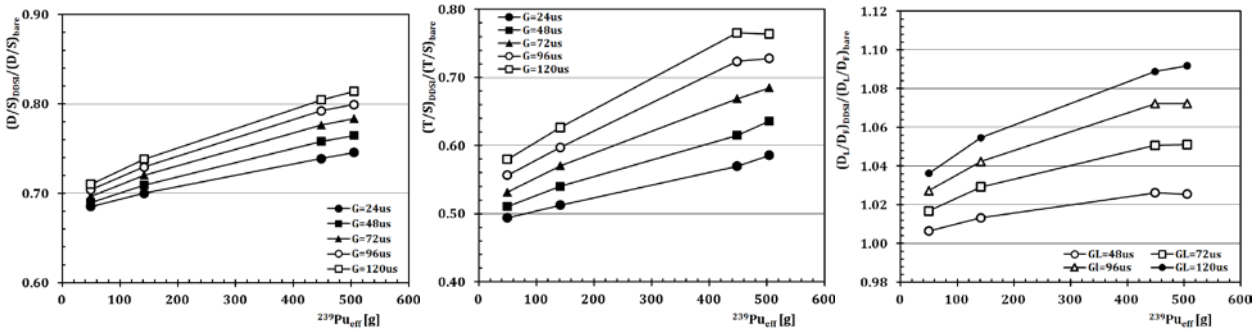

Fig.9 *Ratios of DDSI signatures as calculated for DDSI and bare geometries.*

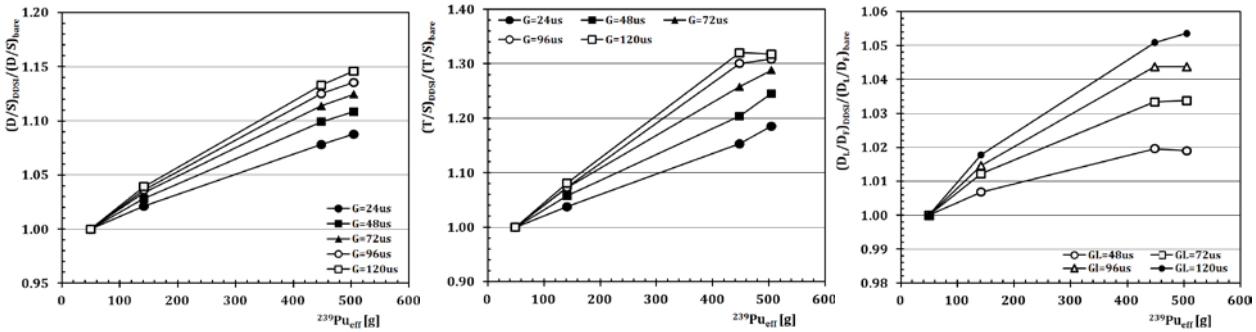

Fig.10 *Normalized ratios of DDSI signatures as calculated for DDSI and bare geometries.*

Overall all three plots in Fig. 10 seem to imply that the longer the gate the higher the sensitivity of the observable, which may saturate only in very late times when all the neutrons eventually die out. On the other hand, the increased sensitivity with longer gates may be more than compensated by decreasing statistics. In order to quantify the influence of both effects we have calculated the uncertainty of the $^{239}Pu_{eff}$ mass determination stemming from the statistical uncertainty of DDSI signatures using dependencies displayed in Fig. 7 as the calibration curves.

Table 6 displays the relative statistical uncertainties of the $^{239}Pu_{eff}$ determination based on the evaluation of D/S and T/S ratio, while **Table 7** displays the same quantity for the D_L/D_F ratio. The values in bold letters indicate the lowest uncertainty for the individual sample and observable used. Comparing the results for D/S and T/S we can conclude that the enhance sensitivity of T/S ratio is in our case compensated by reduced statistics and T/S thus does not provide for more accurate $^{239}Pu_{eff}$ evaluation than D/S. Moreover, despite the additional M_{th} provided by the HDPE container and the resulting increase of correlated neutron flux in late time domains, it is still the traditional short gate widths (i.e. 24μs) which lead to the most accurate results, especially for the samples of more than 100g of Pu, although the smallest PuO_2 assay can benefit from longer gates of 48μs in case of D/S. The uncertainties in $^{239}Pu_{eff}$ determination achieved with D_L/D_F are consistently and significantly higher than in case of D/S and T/S. But unlike the other two ratios, the D_L/D_F benefits strongly from longer G_L and perhaps widths greater than 120μs (i.e. limit of the current study) may provide for better results, even though the trends observable in Table 7 seem to suggest saturation of the uncertainty just around G_L=120μs. It is also apparent that D_L/D_F does not seem to perform well in assays of smaller quantities of Pu with small multiplication, but significantly improves with increasing $^{239}Pu_{eff}$ mass and/or multiplication.

Table 6 *Statistical uncertainty in $^{239}Pu_{eff}$ determination using D/S and T/S ratio (in [%])*

	D/S				T/S			
Item / **G [μs]**	**LAO250**	**LAO251**	**LAO253**	**LAO255**	**LAO250**	**LAO251**	**LAO253**	**LAO255**
24	3.88	**2.18**	**0.39**	**0.71**	**4.30**	**1.85**	1.15	**0.89**
48	**3.65**	2.33	0.54	0.72	**4.30**	2.43	**1.07**	1.21
72	4.14	2.40	0.60	0.89	6.06	2.90	1.27	1.73
96	4.19	2.68	0.70	0.90	7.00	3.03	1.47	1.82
120	4.23	2.89	0.76	0.86	7.36	3.12	1.95	2.62

Table 7 *Statistical uncertainty in $^{239}Pu_{eff}$ determination using D_L/D_F ratio (in [%])*

	D_L/D_F			
Item / **G_L [μs]**	**LAO250**	**LAO251**	**LAO253**	**LAO255**
48	87	51.9	9.7	21.0
72	50.7	29.9	6.08	12.1
96	41.4	24.9	5.24	8.85
120	**34.3**	**23.2**	**4.85**	**4.96**

Discussion

In the previous section the performance of the DDSI based assay/verification system was evaluated. It appears that the method based on D/S and possibly T/S can be of practical use for the treaty verification purposes, although it should not be forgotten that several important and relevant aspects of potential Pu material to be verified could not be addressed within this study. As already discussed above, relative contributions of fertile and fissile isotopes to the measured signal in case of D/S and T/S cannot be quantified unless isotopically diverse samples are included in the study. It also remains to be understood how various geometry and chemical, as well as physical properties of the sample or perhaps even lack of such knowledge may influence the overall results, since the multiplication clearly depends on such properties, and, in turn, the DDSI signatures depend on the multiplication. Moreover, it is not yet clear how important the role of the self-shielding effects, typical for thermal neutrons observed in very late gates (Fig. 4), will be in case of Pu samples of kg quantities expected in the treaty verification process. A follow-up study (simulation) addressing the above mentioned issues is necessary in order to fully explore and evaluate the potential of the DDSI method.

Summary

Within this study, we have performed an experimental and simulation study of DDSI effect in four PuO_2 samples of almost identical isotopic composition with total Pu mass ranging from 60 to 614g. In the experimental part of the project we have used the ENMC detector modified by an inserted HDPE cylinder to induce a DDSI effect in the sample. We have found that all three proposed DDSI signatures (D/S, T/S, and D_L/D_F) yield sensitivity to the Pu content in the sample, yet due to the dedicated Monte Carlo simulations we found that only the D_L/D_F observable is exclusively sensitive to the fissile content of the sample, while the D/S and T/S observables contain contributions from both the fertile as well as the fissile isotopes present.

We have evaluated the uncertainties in determination of $^{239}Pu_{eff}$ content using all three proposed DDSI signatures. We found that in case of the D/S and T/S ratios the lowest uncertainties are achieved with a rather short gate of 24μs for the samples containing more than 100g of Pu, but longer gates (72-96μs) lead to lower uncertainty in the case of assay of smaller samples. The D_L/D_F signature performs best with G_F=24μs and G_L=120 μs or longer, but overall this observable does not seem to be suitable for assay of small Pu samples (<100g). Its performance improves significantly with increasing Pu content and multiplication.

Considering the results and statistical uncertainties of the Monte Carlo simulations equivalent to 900s assay with the ENMC detector in DDSI configuration and depending on the total Pu content in the sample we were able to reconstruct the $^{239}Pu_{eff}$ content with statistical uncertainty of 0.4-3.7% in case of D/S ratio, 1.1-4.3% in case of T/S ratio, and 4.9-34.3% in the case of the D_L/D_F.

References

[1] J. T. Caldwell et al., "*Apparatus and method for quantitative assay of generic transuranic wastes from nuclear reactors*," US Patent No. 363,979, (1982).

[2] H.O. Menlove, S.H. Menlove, and S.J. Tobin: "Fissile and Fertile nuclear material measurements using a new differential die-away self-interogation technique", Nucl. Inst. and Meth. A 602 (2009), p. 588-593

[3] H.O. Menlove, C.D. Rael, K.E. Kroncke, and K.J. DeAguero: "*Manual for the Epithermal Neutron Multiplicity Detector (ENMC) for Measurement of Impure MOX and Plutonium Samples*", LANL internal report LA-14088, May 2004.

[4] Pelowitz, J. F. (Ed.). 2005. MCNPXTM User's Manual Version 2.5.0, Los Alamos National Laboratory report LA-CP-05-0369

[5] Martyn Swinhoe and Rollin Lakis, *private communications*